HHS Public Access

Author manuscript

Shock. Author manuscript; available in PMC 2024 April 01.

Published in final edited form as:

Shock. 2023 April 01; 59(4): 612–620. doi:10.1097/SHK.0000000000002081.

Myosin light chain kinase deletion worsens lung permeability and increases mortality in pneumonia-induced sepsis

Deena B. Chihade[1,2], **Prestina Smith**[3], **David A. Swift**[1,2], **Shunsuke Otani**[1,2], **Wenxiao Zhang**[1,2], **Ching-Wen Chen**[1,2], **Lauren A. Jeffers**[3], **Zhe Liang**[1,2], **Takashi Shimazui**[1,2], **Eileen M. Burd**[4], **Alton B. Farris**[4], **Bashar S. Staitieh**[2,3], **David M. Guidot**[3], **Mandy L. Ford**[1,5,6], **Michael Koval**[3,6], **Craig M. Coopersmith**[1,2,6]

[1]Department of Surgery; Emory University School of Medicine; Atlanta, GA

[2]Emory Critical Care Center; Emory University School of Medicine; Atlanta, GA

[3]Division of Pulmonary, Allergy, Critical Care, and Sleep Medicine; Emory University School of Medicine; Atlanta, GA,

[4]Department of Pathology and Laboratory Medicine; Emory University School of Medicine; Atlanta, Georgia, 30322

[5]Emory Transplant Center; Emory University School of Medicine; Atlanta, Georgia

[6]This work reflects equal contributions from these authors' laboratories

Abstract

Increased epithelial permeability in sepsis is mediated via disruptions in tight junctions, which are closely associated with the peri-junctional actin-myosin ring. Genetic deletion of myosin light chain kinase (MLCK) reverses sepsis-induced intestinal hyperpermeability and improves survival in a murine model of intra-abdominal sepsis. In an attempt to determine the generalizability of these findings, this study measured the impact of MLCK deletion on survival and potential associated mechanisms following pneumonia-induced sepsis. $MLCK^{-/-}$ and wild type (WT) mice underwent intratracheal injection of *Pseudomonas aeruginosa*. Unexpectedly, survival was significantly worse in $MLCK^{-/-}$ mice than WT mice. This was associated with increased permeability to Evans Blue dye in bronchoalveolar lavage (BAL) fluid but not in tissue homogenate, suggesting increased alveolar epithelial leak. Additionally, bacterial burden was increased in BAL fluid. Cytokine array using whole lung homogenate demonstrated increases in multiple pro- and anti-inflammatory cytokines in knockout mice. These local pulmonary changes were associated with systemic inflammation with increased serum levels of IL-6 and IL-10 and a marked increase in bacteremia in $MLCK^{-/-}$ mice. Increased numbers of both bulk and memory $CD4^{+}$ T cells were identified in the spleens of knockout mice, with increased early and late activation. These results demonstrate that genetic deletion of MLCK unexpectedly increases mortality in pulmonary sepsis, associated with worsened alveolar epithelial leak and both local and

Address correspondence to: Craig Coopersmith, 101 Woodruff Circle, Suite WMB 5105, Atlanta, GA 30322, Phone: (404) 727-4273, Fax: (404) 727-3660, cmcoop3@emory.edu.

Disclosure statement: The authors have nothing to disclose.

systemic inflammation. This suggests that caution is required in targeting MLCK for therapeutic gain in sepsis.

Keywords

Tight junction; *Pseudomonas aeruginosa* ; mice; leak; bronchoalveolar lavage; cytokines; inflammation

INTRODUCTION

Sepsis is life-threatening organ dysfunction caused by a dysregulated host response to infection (1). Sepsis is a global health emergency as it was responsible for nearly 20% of deaths in the world prior to the COVID-19 pandemic (2). In addition, costs for Medicare beneficiaries exceed $60 billion in the United States alone (3). However, despite the significant morbidity and mortality attached to sepsis, no targeted therapies are available once antibiotics and supportive care are unsuccessful (4).

Permeability is increased in both the epithelium and endothelium following sepsis and this is associated with increased mortality (5–8). Myosin light chain kinase (MLCK) phosphorylates the myosin regulatory light chain, leading to cytoskeleton contraction and tight junction regulation (9). MLCK is widely distributed on a variety of cell types including vascular endothelium, epithelium in multiple tissues, T lymphocytes and smooth muscle (10–15). Microbial infections activate MLCK, which increases permeability via tight junctions (16, 17). This can be exacerbated by production of pro-inflammatory cytokines induced by MLCK, which further increases permeability and activates MLCK (18, 19). Notably, these changes can be reversed via MLCK inhibition (20).

Based upon its impact on permeability, MLCK inhibition has been proposed as a therapeutic target in critical illness. Supporting the potential efficacy of this approach, two groups have shown that $MLCK^{-/-}$ mice have improved gut permeability and improved survival following cecal ligation and puncture, a model of polymicrobial sepsis, associated with a marked decrease in systemic interleukin (IL)-10 and late activation in the immune system with decreased $CD4^{+}CD25^{+}$ and $CD8^{+}CD25^{+}$ T cells (21, 22). In addition, $MLCK^{-/-}$ mice are less susceptible to critical illness caused by sterile inflammation as knockout mice have decreased lipopolysaccharide (LPS)-induced acute lung injury, associated with improved survival following mechanical ventilation (23). Inhibitor studies of MLCK have yielded mixed results. A small molecule inhibitor of MLCK protected wild type (WT) mice from LPS-induced lung injury and death (23). In contrast, two different MLCK inhibitors either paradoxically increased gut permeability and mortality or failed to alter survival in WT mice in a model of cecal ligation and puncture (24).

The success rate in clinical trials for sepsis has been poor with no conclusive evidence that any pharmacologic interventions have improved survival (25). While the reasons behind this are assuredly multifactorial, one likely reason has been that clinical trials combine all septic patients together, despite differences in both inciting organism and host response seen in patients and in pre-clinical trials (26–31). Thus, while genetic deletion of MLCK has been

shown to improve survival in intraabdominal sepsis and in sterile inflammation, we sought to see how generalizable these findings might be by examining MLCK$^{-/-}$ mice subjected to *Pseudomonas aeruginosa* pneumonia. Unexpectedly, mortality was markedly increased with increased lung epithelial permeability and evidence of increased local and systemic inflammation and infection.

MATERIALS AND METHODS

Animals

Eight- to 12-week old male and female mice with a genetic deletion of the long isoform of MLCK (MLCK210) on a mixed 129/C57Bl/6J background (a generous gift from Dr. Martin Watterson, Northwestern University) were utilized for all experiments (23, 32). Mice were bred to genetically identical animals (i.e. MLCK$^{-/-}$ to MLCK$^{-/-}$ and WT to WT). Mice were housed in the Division of Animal Resources (DAR) at Emory University and kept on a strict day/night light cycle. Animals were given free access to food and water throughout the course of all experiments. In addition to age- and gender-matching, mice also had room- and rack-matching. Experiments were performed in accordance with the National Institutes of Health Guidelines for the Use of Laboratory Animals and were approved by the Institutional Animal Care and Use Committee at Emory University School of Medicine (protocol DAR-201800033).

Preparation of Inoculum

Culti-loops of *P. aeruginosa* ATCC 27853 (Remel Microbiology Products, Thermo Scientific, Lenexa, KS) were dissolved in tryptic soy broth to create aliquot stocks containing 10 ul of bacteria maintained in 15% glycerol for storage at −80°C. Frozen aliquots were thawed and cultured overnight on blood agar to create colonies. Colonies were subcultured and grown overnight in constant-motion tryptic soy broth at 37°C in ambient air and then centrifuged for 15 minutes at 4000 × g. The resulting pellet was resuspended in sterile saline and centrifuged again. The final density of the inoculum was adjusted to 0.19A 600nm, corresponding to a cell density of approximately 2× 10^8 colony-forming units (CFU)/mL as determined by serial dilution and colony counts.

Sepsis Model

Under isoflurane anesthesia (4% induction and 2% intra-procedural maintenance), mice were placed in supine position on a subscapular bump for neck extension. After shaving and prepping the animals, an approximate 0.5 cm longitudinal incision was made overlying the cervical portion of the anterior neck. Dissection was carried down through the subcutaneous tissue, and strap muscles were divided with gentle traction. Animals received an intratracheal injection of 40 μl of *P. aeruginosa*. Based on the cell density and volume injected, the dose administered to each animal was between twenty and forty million CFUs per injection. Tissues were then re-approximated and skin closure performed using skin glue. Mice were held vertically for 10 seconds to facilitate the delivery of bacteria into the lung. Mice received a 1 ml sterile normal saline bolus administered subcutaneously for fluid resuscitation. All mice also received a subcutaneous injection of buprenex (0.1 mg/kg;

McKesson Medical, San Francisco, CA.) prior to incision. Mice were either sacrificed 24 hours post-operatively or monitored for 7 days for survival.

PIK administration

Mice were randomized to receive either membrane permeant inhibitor of MLCK (PIK, 50μM, Calbiochem Millipore Sigma, Billerica, MA) or an equivalent volume of vehicle via intraperitoneal injection beginning post-operatively and then continued every 12 hours.

Evans Blue Permeability Assay

Mice received an injection of 200 ul of 0.5% Evans Blue in sterile PBS into the lateral tail vein and were sacrificed one hour later when BAL, lung tissue and blood were collected. Lung samples were weighed then incubated in 250 ul of formamide in a 55°C bath for 48 hours. Blood was centrifuged at 1500 × g for 15 min for collection of serum. Evans Blue in BAL, lung tissue extracts and blood underwent spectrophotometric analysis at 620 nm (33). Lung-specific tissue-specific turbidity correction factor was utilized according to Moitra et al. BAL and tissue extracts were analyzed at 740 nm, with the correction factor of $y = 1.193x + 0.007$ applied to raw spectrophotometric data with subsequent normalization to serum prior to statistical analysis (34). Values are displayed as ng of extravasated Evans Blue per mL of BAL or mg of tissue.

Histologic Analysis

Immediately after sacrifice, entire right lung lobes were excised and placed in ice-cold 10% buffered formalin for fixation at 4°C for 48 hours. Samples were submitted to the Emory Histology Core for paraffin-embedding and sectioning. Images were collected on a Nikon Elements microscope using Imaging Software-EIS Elements BR 3.10 (Nikon Instruments, Melville, NY). Lung histology was examined by a pathologist (ABF) blinded to sample identity. Lung histology was scored based upon proportion of tissue with inflammation as follows: no inflammation (0), 1–4% (1), 5–10% (2), 11–20% (3), 21–100% (4).

Lung Cytokine Array Analysis

Whole left lung lobes were excised immediately after sacrifice, flash frozen and homogenized in 2 ml PBS with cOmplete Mini protease inhibitor cocktail (Sigma-Aldrich, St. Louis, MO). Samples were frozen at −20°C overnight with Triton X-100. Samples were then thawed and centrifuged at 10,000 g for 5 minutes. Supernatants were collected and a standard Bradford assay was used to measure protein concentration within each lysate sample. Pooled purified protein lysates were analyzed by the Proteome Profiler Mouse Cytokine Array Kit (Panel A, R&D Systems, Minneapolis, MN). Array chemiluminescent reaction was captured and quantified by FIJI/ImageJ (National Institutes of Health, Bethesda, MD).

Multiplex Cytokine Analysis

BAL fluid, lung tissue and serum were collected at the time of sacrifice and then centrifuged at 5,000 rpm for 5 min. Concentrations of interleukin (IL)-1β, IL-2, IL-6, IL-10, IL-4, IL-12, IL-13, IFN-γ, TGF-β and TNF in serum samples were measured using a multiplex cytokine

assay (Bio-Rad, Hercules, CA) according to the manufacturer's instructions. All samples were run in duplicate.

Bacterial Cultures

BAL and serum fluid samples were obtained for bacterial culture at the time of sacrifice. The tracheobronchial tree with catheterized with a 22 gauge angiocatheter (Becton, Dickson and Co., Ontario, Canada). Air was suctioned from the airway and one ml of sterile PBS was infused through the catheter employing external thoracic massage. Re-infusion and withdraw were performed twice to complete a proper lavage, prior to collection and placement onto ice. In addition, blood was obtained by intracardiac puncture. All samples were spun down for 10 min at 19,000 rpm prior to plating. Quantitative cultures were done by preparing serial 10-fold dilutions of the specimen in sterile saline. The original sample and each dilution were inoculated onto sheep blood agar plates (Remel, San Diego, CA) and incubated at 37°C in ambient air for 24 hours at which time colony counts were enumerated.

Myeloperoxidase activity

BAL fluid was centrifuged at 5,000 rpm for 5 min. Lung tissue was snap-frozen in liquid nitrogen immediately after sacrifice. Tissue was weighed, thawed and placed in lysis buffer containing protease inhibitor cocktail (0.5% Triton X-100, 10 mM EDTA, 100 mM NaCl, 50 mM Tris HCl) at a ratio of 5 ml for every 1 mg of tissue. Following addition of substrate buffer containing O-dianisidine and 0.0005% hydrogen peroxide, myeloperoxidase (MPO) activity was measured at 460 nm wavelength over 6 min (Bio-Tek Instruments Quant Microplate Spectrophotometer, Winooski, VT). MPO activity was calculated as optical density/minute/mg of lung tissue or per μL of BAL fluid.

Flow Cytometric Analysis and Staining

Spleens were collected and analyzed via flow cytometry as previously described (35). Splenic tissue was homogenized through a 70-mm pore strainer to create single cell suspensions in FACS buffer. Cell suspensions were treated with fluorescent Zombie Orange™ dye (live/dead stain) for 15 min at room temperature. Anti-CD16/CD32 antibody (clone 2.4G2) was used to block Fc receptors. Accucheck Counting beads (Thermo Fisher Scientific) were added to each sample before data collection to calculate the absolute number of cells per spleen. All data was analyzed with FlowJo software (Tree Star, Ashland, OR, USA).

Macrophage Phagocytic Analysis

Alveolar macrophages were incubated with fresh culture medium plus 1×10^6 pHrodo red *Staphylococcus aureus* BioParticles at 37°C, 5% CO_2 in the dark. After culture for 2 hours, the bioparticles were removed, washed twice with PBS, and 0.04% Trypan blue solution was added for 2 min to quench the remaining fluorescence outside the cells. Cells were then washed with PBS prior to fixation with 4% paraformaldehyde. To measure quantitative phagocytosis, fluorescent digital images were captured with identical settings by a fluorescence microscope (Olympus America, Center Valley, PA) and analyzed with ImageJ

software. Bacterial phagocytosis was expressed as relative fluorescence intensity and reflects the number of *S. aureus* bioparticles phagocytosed per cell.

Statistical Analysis

Data analysis was performed using the statistical software program Prism 6.0 (GraphPad, San Diego, CA). Data are presented as mean ± standard error of the mean. Data were tested for Gaussian distribution using the D'Agostino-Pearson omnibus normality test. Comparison between groups with a Gaussian distribution was performed using the Students *t* test. Comparison between groups that did not have a Gaussian distribution was performed using the Mann-Whitney test. Survival was analyzed using the log-rank test. A p value <0.05 was considered to be statistically significant.

RESULTS

Mortality, lung permeability and bacterial burden are increased in MLCK$^{-/-}$ mice following pneumonia

WT and MLCK$^{-/-}$ mice underwent intratracheal injection of *P. aeruginosa* and were followed for 7-day survival. Survival of MLCK$^{-/-}$ mice unexpectedly decreased markedly between 48 and 72 hours after pneumonia (Fig. 1A). To determine if pharmacologic inhibition of MLCK yielded similar results, WT were randomized to receive either PIK or vehicle after the induction of pneumonia. A trend towards increased mortality was seen in mice treated with pharmacologic MLCK inhibition (Fig. 1B).

All subsequent analysis was performed 24 hours post-pneumonia. This timepoint was chosen for detailed analysis since at this stage multiple elements of the host response are maximally altered by sepsis while the mice remained viable. One hour prior to sacrifice, mice were injected with Evans Blue and then serum, BAL, and lung tissue was collected. Prior to spectrophotometric measurement, gross imaging of plated BAL and pulmonary tissue extracts containing varying concentrations of Evans Blue were obtained. A visible increase in Evans Blue was noted in BAL fluid of septic MLCK$^{-/-}$ mice compared to WT mice (Fig. 2A). Normalized to serum, BAL permeability was significantly higher in septic MLCK$^{-/-}$ mice (Fig. 2B). Permeability in the pulmonary tissue compartment was not statistically different in septic MLCK$^{-/-}$ mice (Fig. 2C). Bacterial burden was also higher in BAL fluid of MLCK$^{-/-}$ mice (Fig. 2D).

Lung hemorrhage and endothelialitis are increased in MLCK$^{-/-}$ mice

Gross examination of lungs revealed that pneumonia induced expected edematous changes in WT mice, when compared to unmanipulated WT mice (Fig. 3A,B) and that additional hemorrhagic changes were seen in lungs from MLCK$^{-/-}$ mice subjected to pneumonia (Fig. 3C). H&E staining revealed significantly increased hemorrhage on a macroscopic level in MLCK$^{-/-}$ mice following pneumonia (Fig. 3D). Quantification by a pathologist blinded to sample identity demonstrated increased endothelialitis histologically in MLCK$^{-/-}$ mice following pneumonia (Fig. 3E) as well as a trend toward increased red blood cell infiltration (Fig. 3F, p=0.05). In contrast, a marked decrease in bronchiolar inflammation was identified in MLCK$^{-/-}$ mice (Fig. 3G). No difference was noted in leukocytic infiltration, septal width,

alveolar inflammation or parenchymal infiltration between knockout and WT mice (Fig. 3H–K).

Lung cytokine levels are increased in MLCK$^{-/-}$ mice

Cytokine array analysis of whole lung homogenates from pooled septic MLCK$^{-/-}$ mice and septic WT mice demonstrated visible alterations across several cytokines (Fig. 4A–C). Measurable increases in lung homogenate cytokines were noted across several groups of pro- and anti-inflammatory cytokines including IL-6, −17 −10, −33, −13, granulocyte-macrophage colony stimulating factor (GM-CSF), TNF, chemokine ligand 9 (CXCL9) and eotaxin 1 (CCL-11) (Fig. 4D, E). Additionally, TNF levels were higher in BAL fluid from septic MLCK$^{-/-}$ mice although no differences were noted in IL-2, IL-6 or IL-10 levels (Fig.4F–I). No difference in MPO activity was identified in lung homogenate or BAL (Fig. 4J,K).

To determine whether MLCK$^{-/-}$ mice have a baseline inability to contain infection within the pulmonary compartment, phagocytic function of alveolar macrophages from MLCK$^{-/-}$ mice to *S. aureus* was assessed prior to initiation of sepsis. Despite the increased BAL bacterial burden of *P. aeruginosa* and mortality in MLCK$^{-/-}$ mice, alveolar macrophages in unmanipulated knockout mice demonstrated increased phagocytic function compared to WT mice (Fig. 4L–N).

Serum cytokines and systemic bacterial burden are increased in MLCK$^{-/-}$ mice

Since pneumonia-induced sepsis induces alterations beyond the local milieu of the lung, mice were assayed for systemic alterations by examining serum cytokines and bacterial load. Serum levels of IL −6 and IL −10 were higher and levels of IL-1β trended higher (p=0.05) in septic MLCK$^{-/-}$ mice compared to septic WT mice (Fig. 5A–C) whereas no differences were detected in IL-2, IL-4, IL-12, IL-13, IFN-γ, TGFβ or TNF (Fig. 5 D–J). This alteration in systemic inflammation was associated with a marked increase in bacterial burden in the bloodstream in MLCK$^{-/-}$ mice (Fig. 5K).

CD4^{+} T cell activation is increased in MLCK$^{-/-}$ mice

In order to determine the impact of MLCK deletion on systemic immunity, spleens were assayed by flow cytometry in knockout and WT mice. There was a substantial increase in the total number of CD4^{+} T cells (Fig. 6A). Activation was increased in CD4^{+} T cells in MLCK $^{-/-}$ mice as evidenced by higher numbers of CD4^{+}CD69^{+} and CD4^{+}CD25^{+} T cells (Fig. 6B,C). Further, there was a significant increase in CD4^{+}CD43^{+} T cells (Fig. 6D). The number of both memory (CD44^{hi}) and naïve (CD44^{lo}) CD4^{+} cells were significantly increased in MLCK $^{-/-}$ mice (Fig. 6E,F). No difference was noted in the frequency of CD4^{+} T cells expressing the exhaustion markers PD-1 or 2B4 (Fig. 6G,H). In contrast, there were no differences in the number of CD8^{+} T cells or activation status of these cells (Fig. 7A–C). There was a decrease in CD8^{+}CD43^{+} T cells (Fig. 7D). There was a small increase in CD44^{hi} memory CD8^{+} cells without a statistically significant difference in CD44^{lo} naïve CD8^{+} T cells. (Fig. 7E,F). No difference was noted in the frequency of CD8^{+} T cells expressing the exhaustion markers PD-1 or 2B4 (Fig. 7G,H).

A significant increase in Foxp3^{+} CD4^{+} regulatory T cells was also observed in MLCK $^{-/-}$ mice relative to WT controls. This difference was observed in both CD44^{hi} and CD44^{lo} Foxp3^{+} CD4^{+} Treg (Fig. 8A–C). In contrast, there was no difference noted in the number of B cells (Fig. 8D). With regard to the innate immune system, increases in the number of dendritic cells, neutrophils, and macrophages were observed in MLCK $^{-/-}$ mice relative to WT controls, while there were no differences in the number of natural killer cells (Fig. 8E–H).

DISCUSSION

This study demonstrates that genetic deletion of MLCK results in worsened survival in mice subjected to *P. aeruginosa* pneumonia, associated with increased permeability to Evans Blue dye and increased bacterial burden in BAL fluid. These findings were unexpected given that genetically identical knockout mice exhibited improved intestinal permeability and improved survival in a model of intraabdominal sepsis (21).

A key question from our findings is why there is such a significant discrepancy between MLCK$^{-/-}$ mice after pneumonia and intraabdominal sepsis – with the former leading to markedly worsened mortality and the latter leading to near 100% survival in knockout mice. Further, while MLCK deletion led to worsened pulmonary permeability and higher local bacterial burden in BAL fluid following pneumonia, the same deletion led to improved intestinal permeability without a change in local bacterial burden in peritoneal fluid following cecal ligation and puncture. In contrast to these changes, there was no difference in gut or lung damage caused by infection initiated in the other tissue in MLCK$^{-/-}$ mice as lung injury was not altered by cecal ligation and puncture and gut integrity (as measured by crypt proliferation, crypt apoptosis and villus length – data not shown) was not altered by pneumonia. To understand potential causes of contradictory results seen with different infections, we first examined pulmonary pathology since the initiating site of infection in pneumonia is the lungs. A key role of MLCK is to increase paracellular permeability, and numerous studies have shown that MLCK deletion, inhibition or decreased activation decreases paracellular permeability in multiple cell types (36–40), with the most robust evidence in the vascular endothelium and the intestinal epithelium. Notably, MLCK mediates increased lung vascular endothelial permeability in LPS-induced lung injury (41–44). Further, mice have a marked increase in lung neutrophil infiltration after an intraperitoneal thrombin challenge, which is attenuated in MLCK$^{-/-}$ mice, suggesting that MLCK directly regulates lung inflammation (45). Finally, MLCK knockout or inhibition has played a protective role in multiple models of lung injury including exposures to LPS sourced from *E. coli, Salmonella* and *P. aeruginosa* (23, 42, 43).

Two barriers exist in the lung – the endothelial/vascular and the alveolar epithelial barrier. Intravenous administration of Evans Blue dye can be used to measure the function of both barriers. If the alveolar epithelial barrier remains intact, but the endothelial barrier is breached, dye can permeate into tissue but not into BAL fluid. Alternatively, if Evans Blue levels in BAL are high but tissue homogenate levels are low, then the main source of barrier permeability is alveolar epithelium (with small hotspots of vascular leak). If Evans Blue levels are high in both BAL and tissue, both barriers are seriously breached. Our findings

demonstrated that Evans Blue levels were elevated in BAL without a statistically significant difference in the pulmonary tissue compartment in septic MLCK$^{-/-}$ mice, suggesting increased damage to the alveolar barrier, accompanied by focal vascular damage as indicated by increased pulmonary hemorrhage.

This was unexpected and different from previous studies examining the role of MLCK both in lung permeability and more globally on lung injury. Intravenous delivery of the MLCK inhibitor PIK in two mouse models of inflammatory lung injury (intratracheal administration of LPS and mechanical ventilation with increased tidal volume) produced a dose-dependent attenuation of both LPS-induced lung inflammation and a 50% reduction in alveolar/vascular permeability and leukocyte influx in ventilator-associated lung injury (42). Further, intravenous injections of MLCK silencing RNA, either directly or within ACE antibody–conjugated liposomes to selectively target the pulmonary vasculature selectively, decreased MLCK lung expression and significantly attenuated LPS-induced and ventilation-induced lung inflammation.

These results are also discordant with the improvement in intestinal permeability seen in MLCK$^{-/-}$ mice subjected to intraabdominal sepsis. Although the mediators underlying pulmonary and intestinal permeability are not identical, there are similarities which made the results contained herein surprising. However, the results are consistent with the equally unexpected findings of worsened intestinal permeability and increased mortality after giving PIK following intraabdominal sepsis (46). While we have previously used intraabdominal sepsis to study intestinal permeability, this insult can also induce lung injury. A study of cecal ligation and puncture to induce preclinical septic acute lung injury demonstrated improved survival by NOX4 knockdown associated with attenuated redox-sensitive activation of the CaMKII/ERK1/2/MLCK pathway, and restored expression of endothelial cell tight junction proteins ZO-1 and Occludin to maintain barrier integrity (47). Similarly, NOX4 knockdown in cultured human lung microvascular endothelial cells also reduced LPS-induced CaMKII/ERK1/2/MLCK activation and endothelial cell barrier dysfunction. Nonetheless, MLCK$^{-/-}$ mice challenged with *P. aeruginosa* had significantly higher levels of several pro-inflammatory cytokines than WT controls, most notably TNF which is associated with impaired lung barrier function (48). One implication of our results is that while MLCK inhibition has a protective effect in many sepsis models, direct lung injury to MLCK$^{-/-}$ mice mediated by *P. aeruginosa* caused an exaggerated, deleterious pro-inflammatory response that could not be mitigated by an MLCK-inhibitable barrier protective pathway.

The numerous immune alterations identified in the spleen may by the result of a secondary effect based upon systemic effects that result from the lung. Within the adaptive immune system, the majority of alterations were found in CD4^{+} T cells manifested by an increase in knockout mice in bulk CD4^{+} T cells, early and late activation and CD4^{+}CD43^{+} T cells. T cell activation is generally considered to be a critical component of the host response to sepsis by ultimately allowing the host to fight off invading pathogens. However, increased activation could lead to a hyperinflammatory response, and it is notable that MLCK$^{-/-}$ mice had increased pro-inflammatory cytokines in BAL fluid, lung homogenate and in the blood. It is plausible that the hypercytokinemia seen in knockout mice helped contribute to

mortality. Similarly, an increase in the number of memory $CD4^+$ memory T cells in MLCK $^{-/-}$ mice would ordinarily be considered to be adaptive, but a greater than expected result could lead to a state in which the host "attacks" itself. This is consistent with the numerous histological abnormalities seen in the lungs of $MLCK^{-/-}$ mice. Further, the significant increase in regulatory T cells in MLCK $^{-/-}$ mice potentially indicates a more suppressive milieu, which could help explain the higher bacterial burden in the blood and BAL of $MLCK^{-/-}$ mice -- despite their alveolar macrophages having increased phagocytic function prior to initiation of sepsis. In contrast, the fact that there was no difference between WT and $MLCK^{-/-}$ mice in exhaustion markers suggests that T cell exhaustion did not play a role in the outcomes observed. Finally, increases in multiple cell lineages in the innate immune system in MLCK $^{-/-}$ mice are also consistent with a pro-inflammatory state which could have been maladaptive in terms of a too robust host response. A complementary potential mechanism relates to the known role of MLCK in T cell migration. MLCK inhibition substantially reduces the probability of T cells climbing sharp-edged ramp-like structures following their experimental fabrication suggesting MLCK activity may be important for T cells to access inflamed tissues with abrupt topographical changes (15). This could help explain why $MLCK^{-/-}$ mice would have less T cell access to the lungs which could theoretically explain the higher bacterial burden in knockout mice.

This manuscript has a number of limitations. First, the knockout mice examined have a germline deletion, leading to the absence of MLCK in all cells throughout the course of development. As such, interpretation of our findings must take into account that that MLCK deletion may have an effect on multiple cell types considering how widely expressed it is in the host. Further, since these mice have a lifelong deficiency in MLCK, it is plausible that compensatory mechanisms occurring prior to the onset of sepsis will result in a different outcome to pneumonia than targeting MLCK only after its onset. Next, further studies are required to determine why permeability was altered in a manner different from expected in $MLCK^{-/-}$ mice, both from published literature as well as what we have previously published in knockout mice in an intraabdominal sepsis model. In addition, while we showed an increase in macrophage numbers in $MLCK^{-/-}$ mice, we did not examine macrophage polarization, which may be important given its importance in bacterial phagocytosis and bactericidal activity. We also did not measure permeability either in the intestinal vascular bed or in the perivascular soft tissues. In addition, although we saw increased hemorrhage in $MLCK^{-/-}$ mice, we did not study coagulation in these mice which may have yielded insights in light of MLCK's role in platelet contraction. Finally, our phagocytosis assay was to *S. aureus* and not to *P. aeruginosa*, which was the pathogen that induced pneumonia in these studies. It is not clear whether intrinsic phagocytosis is equivalent to different bacteria, especially since *S. aureus* are native flora in a laboratory mouse (so would be expected to result in pre-existing memory cells) whereas *P. aeruginosa* are not.

Despite these limitations, we identified an increase in mortality in $MLCK^{-/-}$ mice subjected to pneumonia-induced sepsis that is paradoxical based upon prior studies with these animals. Additional work needs to be done to explain these unexpected findings and which of the multiple differences between WT and $MLCK^{-/-}$ mice are responsible for worsened survival. In conjunction with increased mortality seen with MLCK inhibition in an intraabdominal sepsis model, these results demonstrate a need to consider how cellular heterogeneity of

MLCK function and diverse etiology influence the progression of disease before MLCK can be considered a viable target for therapy in sepsis.

Acknowledgments

This work was supported by funding from the National Institutes of Health (GM072808, GM095442, AI070081, GM104323, AI149724, HL149323, AA025854, HL137112, GM000680, HL144478, AA025857, AA024512)

REFERENCES

1. Singer M, Deutschman CS, Seymour CW, Shankar-Hari M, Annane D, Bauer M, et al. The Third International Consensus Definitions for Sepsis and Septic Shock (Sepsis-3). JAMA. 2016;315(8):801–10. [PubMed: 26903338]
2. Rudd KE, Johnson SC, Agesa KM, Shackelford KA, Tsoi D, Kievlan DR, et al. Global, regional, and national sepsis incidence and mortality, 1990–2017: analysis for the Global Burden of Disease Study. Lancet. 2020;395(10219):200–11. [PubMed: 31954465]
3. Buchman TG, Simpson SQ, Sciarretta KL, Finne KP, Sowers N, Collier M, et al. Sepsis Among Medicare Beneficiaries: 1. The Burdens of Sepsis, 2012–2018. Crit Care Med. 2020;48(3):276–88. [PubMed: 32058366]
4. Evans L, Rhodes A, Alhazzani W, Antonelli M, Coopersmith CM, French C, et al. Surviving Sepsis Campaign: International Guidelines for Management of Sepsis and Septic Shock 2021. Crit Care Med. 2021;49(11):e1063–e143. [PubMed: 34605781]
5. Wang R, Song W, Xie C, Zhong W, Xu H, Zhou Q, et al. Urinary Trypsin Inhibitor Protects Tight Junctions of Septic Pulmonary Capillary Endothelial Cells by Regulating the Functions of Macrophages. J Inflamm Res. 2021;14:1973–89. [PubMed: 34045879]
6. Yang L, Liu S, Han S, Hu Y, Wu Z, Shi X, et al. The HDL from septic-ARDS patients with composition changes exacerbates pulmonary endothelial dysfunction and acute lung injury induced by cecal ligation and puncture (CLP) in mice. Respir Res. 2020;21(1):293. [PubMed: 33148285]
7. Yoseph BP, Klingensmith NJ, Liang Z, Breed ER, Burd EM, Mittal R, et al. Mechanisms of Intestinal Barrier Dysfunction in Sepsis. Shock. 2016;46(1):52–9. [PubMed: 27299587]
8. Liu Y, Mu S, Li X, Liang Y, Wang L, Ma X. Unfractionated Heparin Alleviates Sepsis-Induced Acute Lung Injury by Protecting Tight Junctions. The Journal of surgical research. 2019;238:175–85. [PubMed: 30771687]
9. Yao Y, Feng Q, Shen J. Myosin light chain kinase regulates intestinal permeability of mucosal homeostasis in Crohn's disease. Expert review of clinical immunology. 2020;16(12):1127–41. [PubMed: 33183108]
10. Sun X, Sun BL, Sammani S, Bermudez T, Dudek SM, Camp SM, et al. Genetic and epigenetic regulation of the non-muscle myosin light chain kinase isoform by lung inflammatory factors and mechanical stress. Clin Sci (Lond). 2021;135(7):963–77. [PubMed: 33792658]
11. Graham WV, He W, Marchiando AM, Zha J, Singh G, Li HS, et al. Intracellular MLCK1 diversion reverses barrier loss to restore mucosal homeostasis. Nature medicine. 2019;25(4):690–700.
12. Rigor RR, Shen Q, Pivetti CD, Wu MH, Yuan SY. Myosin light chain kinase signaling in endothelial barrier dysfunction. Med Res Rev. 2013;33(5):911–33. [PubMed: 22886693]
13. Sorensen DW, Injeti ER, Mejia-Aguilar L, Williams JM, Pearce WJ. Postnatal development alters functional compartmentalization of myosin light chain kinase in ovine carotid arteries. Am J Physiol Regul Integr Comp Physiol. 2021;321(3):R441–r53. [PubMed: 34318702]
14. He WQ, Wang J, Sheng JY, Zha JM, Graham WV, Turner JR. Contributions of Myosin Light Chain Kinase to Regulation of Epithelial Paracellular Permeability and Mucosal Homeostasis. International journal of molecular sciences. 2020;21(3).
15. Song KH, Lee J, Jung HR, Park H, Doh J. Turning behaviors of T cells climbing up ramp-like structures are regulated by myosin light chain kinase activity and lamellipodia formation. Sci Rep. 2017;7(1):11533. [PubMed: 28912435]
16. Meinzer U, Barreau F, Esmiol-Welterlin S, Jung C, Villard C, Leger T, et al. Yersinia pseudotuberculosis effector YopJ subverts the Nod2/RICK/TAK1 pathway and activates caspase-1

to induce intestinal barrier dysfunction. Cell Host Microbe. 2012;11(4):337–51. [PubMed: 22520462]

17. Jung C, Meinzer U, Montcuquet N, Thachil E, Chateau D, Thiebaut R, et al. Yersinia pseudotuberculosis disrupts intestinal barrier integrity through hematopoietic TLR-2 signaling. J Clin Invest. 2012;122(6):2239–51. [PubMed: 22565313]
18. Zahs A, Bird MD, Ramirez L, Turner JR, Choudhry MA, Kovacs EJ. Inhibition of long myosin light-chain kinase activation alleviates intestinal damage after binge ethanol exposure and burn injury. Am J Physiol Gastrointest Liver Physiol. 2012;303(6):G705–G12. [PubMed: 22790598]
19. Yu D, Marchiando AM, Weber CR, Raleigh DR, Wang Y, Shen L, et al. MLCK-dependent exchange and actin binding region-dependent anchoring of ZO-1 regulate tight junction barrier function. Proc Natl Acad Sci U S A. 2010;107(18):8237–41. [PubMed: 20404178]
20. Yuhan R, Koutsouris A, Savkovic SD, Hecht G. Enteropathogenic Escherichia coli-induced myosin light chain phosphorylation alters intestinal epithelial permeability. Gastroenterology. 1997;113(6):1873–82. [PubMed: 9394726]
21. Lorentz CA, Liang Z, Meng M, Chen CW, Yoseph BP, Breed ER, et al. Myosin light chain kinase knockout improves gut barrier function and confers a survival advantage in polymicrobial sepsis. Molecular medicine (Cambridge, Mass). 2017;23:155–65. [PubMed: 28598488]
22. Ralay RH, Carusio N, Wangensteen R, Ohlmann P, Loichot C, Tesse A, et al. Protection against endotoxic shock as a consequence of reduced nitrosative stress in MLCK210-null mice. Am J Pathol. 2007;170(2):439–46. [PubMed: 17255312]
23. Wainwright MS, Rossi J, Schavocky J, Crawford S, Steinhorn D, Velentza AV, et al. Protein kinase involved in lung injury susceptibility: evidence from enzyme isoform genetic knockout and in vivo inhibitor treatment. Proc Natl Acad Sci U S A. 2003;100(10):6233–8. [PubMed: 12730364]
24. Sun Y, Oami T, Liang Z, Miniet AA, Burd EM, Ford ML, et al. Membrane Permeant Inhibitor of Myosin Light Chain Kinase Worsens Survival in Murine Polymicrobial Sepsis. Shock. 2021.
25. Santacruz CA, Pereira AJ, Celis E, Vincent JL. Which Multicenter Randomized Controlled Trials in Critical Care Medicine Have Shown Reduced Mortality? A Systematic Review. Crit Care Med. 2019;47(12):1680–91. [PubMed: 31567349]
26. Wong HR, Cvijanovich NZ, Anas N, Allen GL, Thomas NJ, Bigham MT, et al. Developing a clinically feasible personalized medicine approach to pediatric septic shock. Am J Respir Crit Care Med. 2015;191(3):309–15. [PubMed: 25489881]
27. Davenport EE, Burnham KL, Radhakrishnan J, Humburg P, Hutton P, Mills TC, et al. Genomic landscape of the individual host response and outcomes in sepsis: a prospective cohort study. Lancet Respir Med. 2016;4(4):259–71. [PubMed: 26917434]
28. Seymour CW, Kennedy JN, Wang S, Chang CH, Elliott CF, Xu Z, et al. Derivation, Validation, and Potential Treatment Implications of Novel Clinical Phenotypes for Sepsis. Jama. 2019;321(20):2003–17. [PubMed: 31104070]
29. Seymour CW, Kerti SJ, Lewis AJ, Kennedy J, Brant E, Griepentrog JE, et al. Murine sepsis phenotypes and differential treatment effects in a randomized trial of prompt antibiotics and fluids. Crit Care. 2019;23(1):384. [PubMed: 31779663]
30. Bhavani SV, Carey KA, Gilbert ER, Afshar M, Verhoef PA, Churpek MM. Identifying Novel Sepsis Subphenotypes Using Temperature Trajectories. Am J Respir Crit Care Med. 2019;200(3):327–35. [PubMed: 30789749]
31. Bhavani SV, Wolfe KS, Hrusch CL, Greenberg JA, Krishack PA, Lin J, et al. Temperature Trajectory Subphenotypes Correlate With Immune Responses in Patients With Sepsis. Crit Care Med. 2020;48(11):1645–53. [PubMed: 32947475]
32. Watterson DM, Collinge M, Lukas TJ, Van Eldik LJ, Birukov KG, Stepanova OV, et al. Multiple gene products are produced from a novel protein kinase transcription region. FEBS Lett. 1995;373(3):217–20. [PubMed: 7589469]
33. Radu M, Chernoff J. An in vivo assay to test blood vessel permeability. J Vis Exp. 2013(73):e50062. [PubMed: 23524912]
34. Smith P, Jeffers LA, Koval M. Effects of different routes of endotoxin injury on barrier function in alcoholic lung syndrome. Alcohol. 2019;80:81–9. [PubMed: 31278041]

35. Zhang W, Anyalebechi JC, Ramonell KM, Chen CW, Xie J, Liang Z, et al. TIGIT modulates sepsis-induced immune dysregulation in mice with preexisting malignancy. JCI insight. 2021;6(11).

36. Lan H, Zhang LY, He W, Li WY, Zeng Z, Qian B, et al. Sinapic Acid Alleviated Inflammation-Induced Intestinal Epithelial Barrier Dysfunction in Lipopolysaccharide- (LPS-) Treated Caco-2 Cells. Mediators Inflamm. 2021;2021:5514075. [PubMed: 34539242]

37. Zhan X, Chen W, Chen J, Lei C, Wei L. Telmisartan Mitigates High-Glucose-Induced Injury in Renal Glomerular Endothelial Cells (rGECs) and Albuminuria in Diabetes Mice. Chem Res Toxicol. 2021;34(9):2079–86. [PubMed: 34464088]

38. Zergane M, Kuebler WM, Michalick L. Heteromeric TRP Channels in Lung Inflammation. Cells. 2021;10(7).

39. Qin C, Jiang Y, Chen X, Bian Y, Wang Y, Xie K, et al. Dexmedetomidine protects against burn-induced intestinal barrier injury via the MLCK/p-MLC signalling pathway. Burns. 2021.

40. Chen X, Hu C, Fan X, Wang Y, Li Q, Su YQ, et al. mTOR Inhibition Promotes Pneumonitis Through Inducing Endothelial Contraction and Hyperpermeability. Am J Respir Cell Mol Biol. 2021.

41. Xu J, Gao XP, Ramchandran R, Zhao YY, Vogel SM, Malik AB. Nonmuscle myosin light-chain kinase mediates neutrophil transmigration in sepsis-induced lung inflammation by activating beta2 integrins. Nat Immunol. 2008;9(8):880–6. [PubMed: 18587400]

42. Mirzapoiazova T, Moitra J, Moreno-Vinasco L, Sammani S, Turner JR, Chiang ET, et al. Non-muscle myosin light chain kinase isoform is a viable molecular target in acute inflammatory lung injury. Am J Respir Cell Mol Biol. 2011;44(1):40–52. [PubMed: 20139351]

43. Eutamene H, Theodorou V, Schmidlin F, Tondereau V, Garcia-Villar R, Salvador-Cartier C, et al. LPS-induced lung inflammation is linked to increased epithelial permeability: role of MLCK. Eur Respir J. 2005;25(5):789–96. [PubMed: 15863634]

44. Kempf CL, Sammani S, Bermudez T, Song JH, Hernon VR, Hufford MK, et al. Critical role for the lung endothelial nonmuscle myosin light-chain kinase isoform in the severity of inflammatory murine lung injury. Pulm Circ. 2022;12(2):e12061. [PubMed: 35514774]

45. Fazal F, Bijli KM, Murrill M, Leonard A, Minhajuddin M, Anwar KN, et al. Critical role of non-muscle myosin light chain kinase in thrombin-induced endothelial cell inflammation and lung PMN infiltration. PloS one. 2013;8(3):e59965. [PubMed: 23555849]

46. Sun Y, Oami T, Liang Z, Miniet AA, Burd EM, Ford ML, et al. Membrane Permeant Inhibitor of Myosin Light Chain Kinase Worsens Survival in Murine Polymicrobial Sepsis. Shock. 2021;56(4):621–8. [PubMed: 33606476]

47. Jiang J, Huang K, Xu S, Garcia JGN, Wang C, Cai H. Targeting NOX4 alleviates sepsis-induced acute lung injury via attenuation of redox-sensitive activation of CaMKII/ERK1/2/MLCK and endothelial cell barrier dysfunction. Redox Biol. 2020;36:101638. [PubMed: 32863203]

48. Lucas R, Hadizamani Y, Enkhbaatar P, Csanyi G, Caldwell RW, Hundsberger H, et al. Dichotomous Role of Tumor Necrosis Factor in Pulmonary Barrier Function and Alveolar Fluid Clearance. Front Physiol. 2021;12:793251. [PubMed: 35264975]

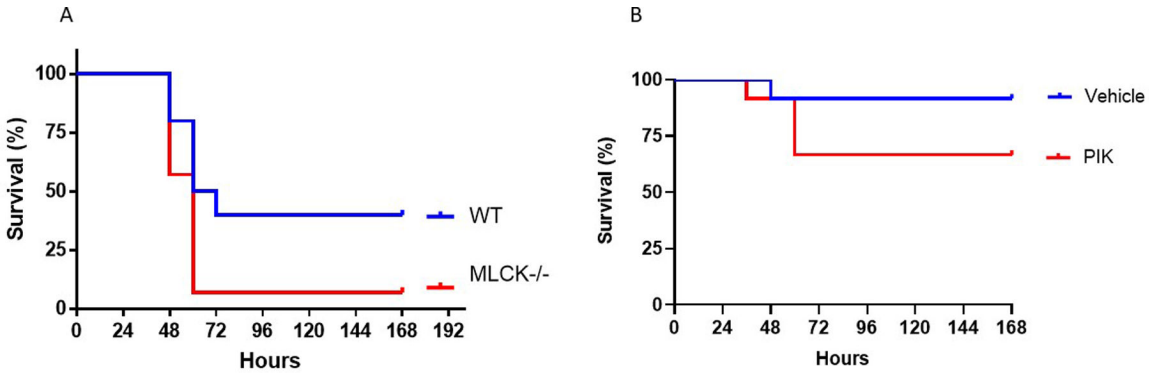

FIG. 1. Mortality following pneumonia.

Survival was significantly worse in MLCK$^{-/-}$ mice seven days after *P. aeruginosa*-induced sepsis (A, n= 14–20/group, p=0.016). A trend toward worsened survival was seen in WT mice given the MLCK inhibitor PIK (B, n=12/group, p=0.16).

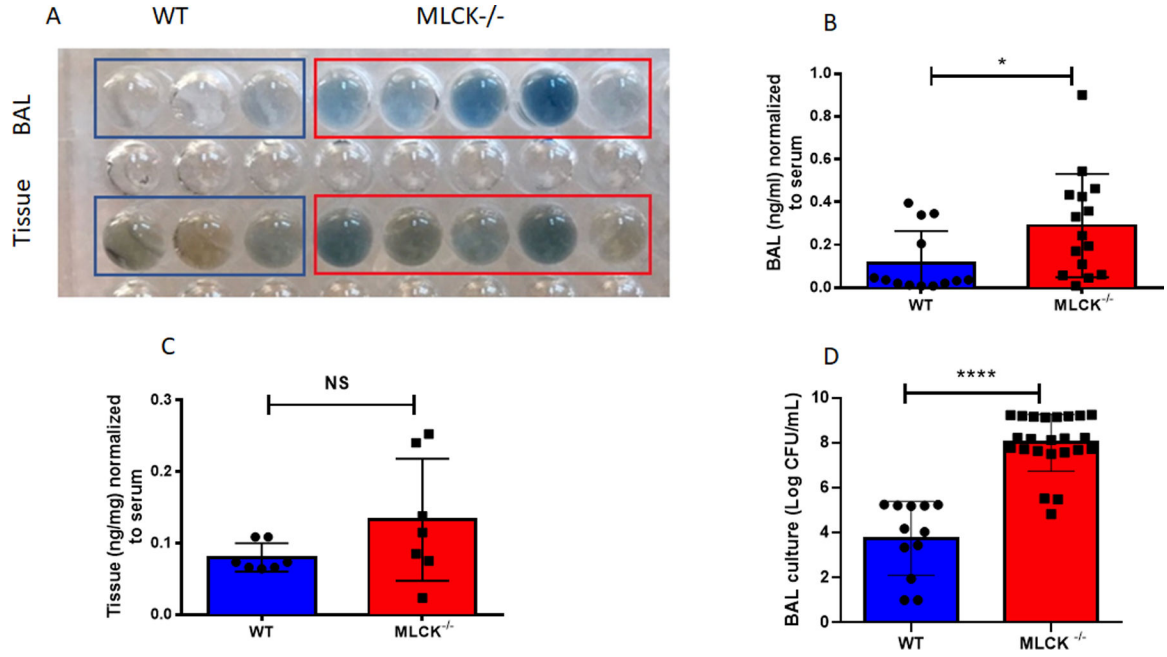

FIG. 2. Lung permeability and bacterial burden following pneumonia.

Imaging of plated BAL and pulmonary tissue shows a visible increase in Evans Blue MLCK$^{-/-}$ mice in BAL fluid (A). BAL permeability was higher in septic MLCK$^{-/-}$ mice (B, n=13–15/group, p=0.03). No statistically significant difference was seen in pulmonary tissue compartment permeability (C, n=7/group, p=0.09). BAL bacterial burden was higher in MLCK$^{-/-}$ mice (D, n=13–23/group, p<0.0001).

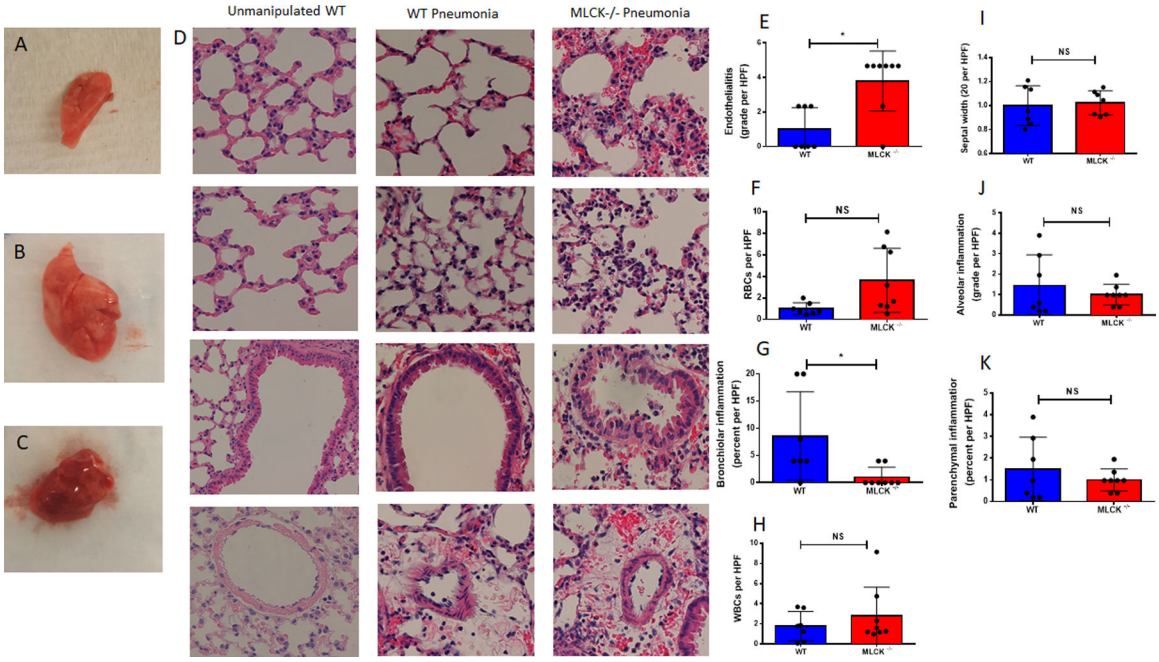

FIG. 3. Lung injury following pneumonia.

Pneumonia induced visible edema in whole lung in WT mice (A unmanipulated, B following pneumonia). Additional hemorrhagic changes were seen in whole lung from MLCK$^{-/-}$ mice following pneumonia (C). These findings were also seen microscopically on H&E stained-lungs (D). Quantification by a blinded pathologist demonstrated increased endothelialitis in MLCK$^{-/-}$ mice compared to WT mice (E, p=0.011) and a trend towards increased red bloods cells (F, p=0.05). Knockout mice also had decreased bronchiolar inflammation (G, p=0.018). No difference was noted in leukocyte infiltration (H, p=0.78), septal width, (I, p= 0.90), alveolar inflammation (J, p=0.89) or parenchymal infiltration (K, p=0.97) between MLCK$^{-/-}$ and WT mice n=7–8/group for all except n=7/group for septal width.

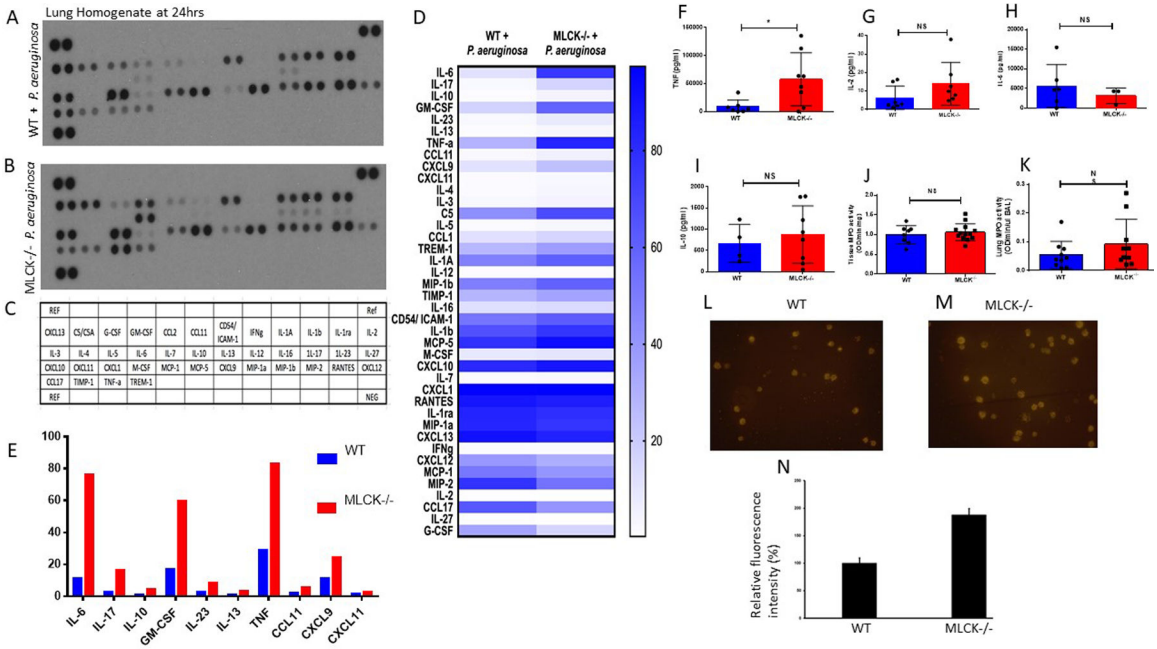

FIG. 4. Lung cytokines and phagocytic capacity.

Cytokine array using whole lung homogenate from pooled septic animals demonstrated alterations across multiple cytokines between WT and MLCK$^{-/-}$ mice (A,B, identity of each cytokine analyzed C). Measurable fold increases in lung homogenate cytokines were noted for multiple cytokines (D with largest fold changes noted in E). BAL levels of TNF were higher in MLCK$^{-/-}$ mice (F, n=7–8/group. p=0.04). No differences were noted in BAL IL-2 (G, n=7/group. p=0.07), IL-6 (H, n=3–6/group, p=0.48) or IL-10 levels (I, n=4–8/group. p=0.93). No differences were detected in MPO activity in either lung homogenate (J, n=8–13/group. p=0.55) or BAL (K, n=9–10/group. p=0.10). Alveolar macrophages in MLCK$^{-/-}$ mice had increased phagocytic to *S. aureus* (L, M raw images in both WT and knockout mice, N, relative fluorescent intensity, n=5–6/group, p<0.0001).

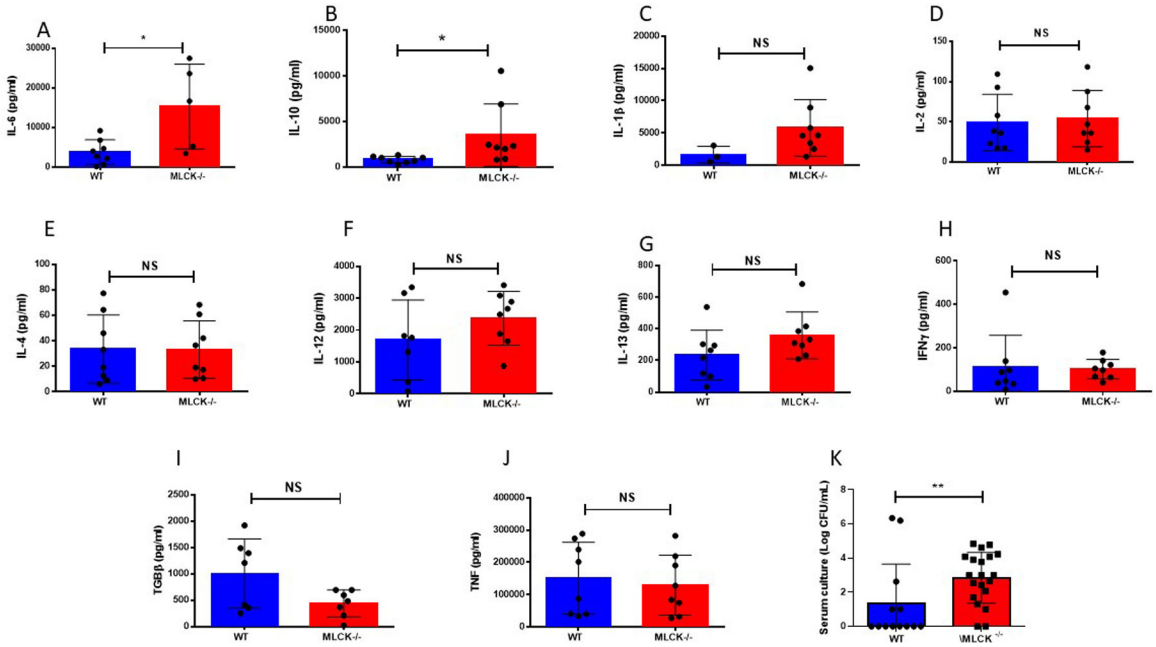

FIG. 5. Serum cytokines and bacterial load after pneumonia.

Serum levels of IL −6 (A, n=5–8/group, p=0.04) and IL −10 (B, n=8/group, p=0.01) were higher in MLCK$^{-/-}$ mice. No differences were noted in L-1β (C, n=3–8/group. p=0.05), IL-2 (D, n=8/group. p=0.78), IL-4 (E, n=8/group, p=0.98), IL-12 (F, n=7–8/group. p=0.34), IL-13 (G, n=8/group. p=0.09), IFN-γ (H, n=8/group, p=0.29), TGFβ (I, n=7/group, p=0.19) or TNF (n=8/group. p=0.69). Bacterial load was also higher in the bloodstream in MLCK$^{-/-}$ mice following pneumonia (K, n=13–20/group, p=0.009).

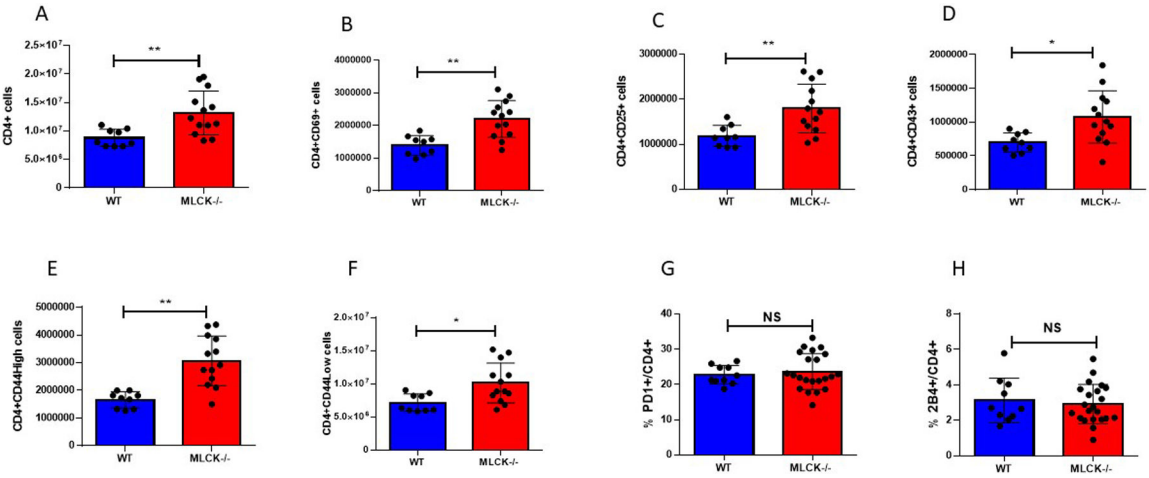

FIG. 6. CD4^{+} T cells after pneumonia

Splenic CD4+ T cells were increased in knockout mice (A, p=9–13/group, p=0.004). Activation was increased in MLCK$^{-/-}$ mice both early as measured by CD4^{+}CD69^{+} (B, p=0.0008) and late as measured by CD4^{+}CD25^{+} T cells (C, p=0.005). There was also an increase in CD4+CD43^{+} T cells (D, p=0.01). The number of both memory CD4^{+}CD44^{hi} T cells (E, p=0.0002) and naïve CD4^{+}CD44^{lo} T cells were also increased in MLCK$^{-/-}$ mice (F, p=0.01). No difference was noted in the exhaustion markers PD-1 (G, p=0.58), or 2B4 (H, p=0.65) on CD4+ T cells. N=9–13/group A-F, n=10–22/group G, H.

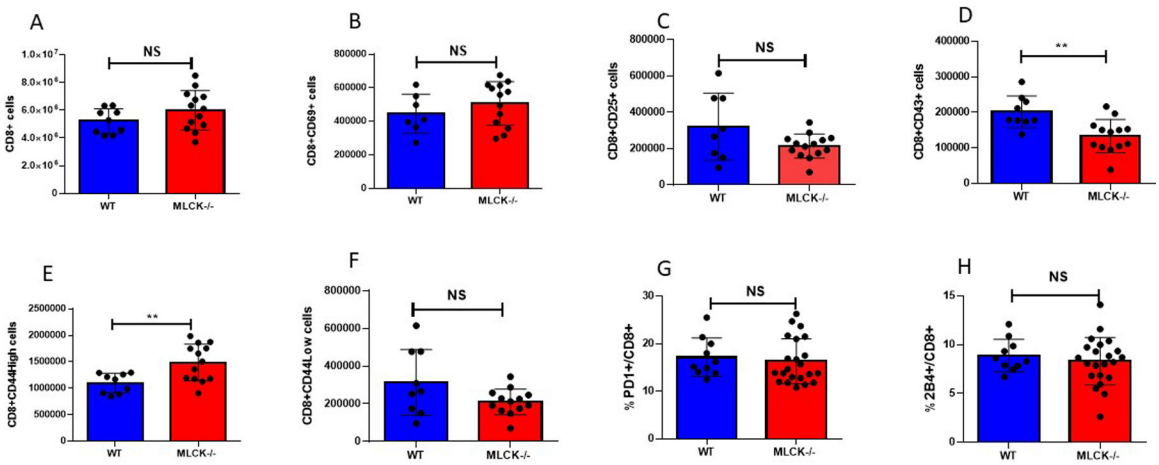

FIG. 7. CD8$^+$ T cells after pneumonia

No difference in CD8$^+$ T cells were detected between WT and knockout mice (A, p=0.16). Neither early (B, p=0.31) nor late (C, p= 0.06) CD8+ T cells activation was altered although a decrease was seen in CD8$^+$CD43$^+$ cells in MLCK$^{-/-}$ mice (D, p=0.003). The number of memory CD8$^+$CD44^{hi} T cells was increased in MLCK$^{-/-}$ mice (E, p=0.006) without a significant change in naïve CD8$^+$CD44l^o T cells (F, p=0.07). No difference was noted in the exhaustion markers PD-1 (G, p=0.62) or 2B4 (H, p=0.49) on CD8+ T cells. N=9–13/group A, B, D-F, n=8–14/group C, n=10–22/group G, H.

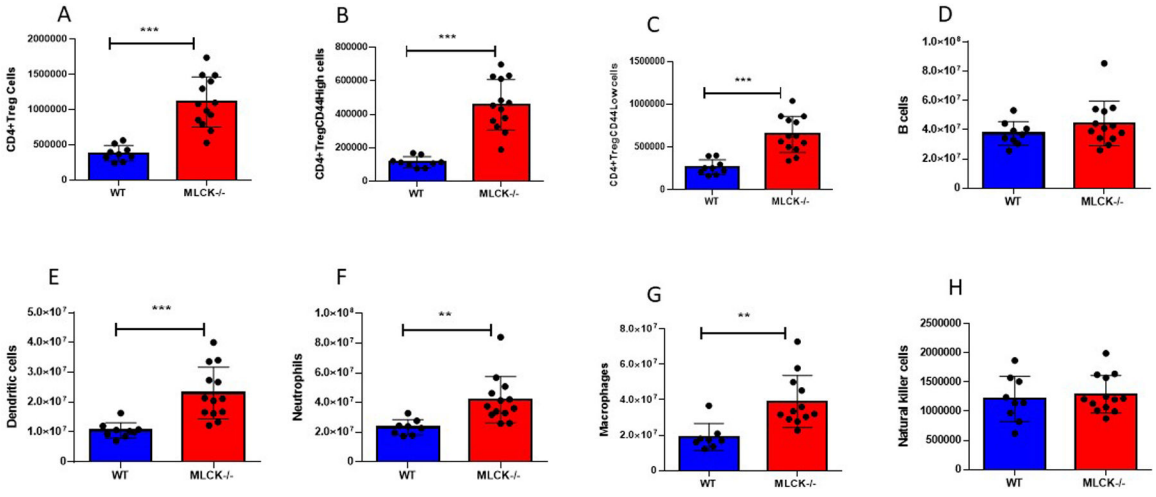

FIG. 8. CD4^{+} T regulatory cells and the innate immune system after pneumonia

The number of regulatory CD4^{+}T cells was increased in MLCK$^{-/-}$ mice (A, p<0.0001). This increase was seen in both CD44^{hi} (B, p<0.0001) and CD44^{lo} Treg cells (C, p<0.0001). No difference was noted in B cells between WT and knockout mice (D, p=0.23). In the innate immune system, dendritic cells (E, p<0.0001), neutrophils (F, p=0.0002), and macrophages (G, p=0.0001) were all increased in MLCK$^{-/-}$ mice while natural killer cells were similar between WT and knockout mice (H, p=0.55), n=9–13/group A-F, H, n=8–12/group G.